Journal of Magnetism and Magnetic Materials 503 (2020) 166603

Contents lists available at ScienceDirect

Journal of Magnetism and Magnetic Materials

journal homepage: www.elsevier.com/locate/jmmm

Research articles

Magnetic properties of $EuFeAs_2$ and the 14 K superconductor $EuFe_{0.97}Ni_{0.03}As_2$

Mohammed A. Albedah[a,b], Zbigniew M. Stadnik[a,*], Olha Fedoryk[a], Ya-Bin Liu[c], Guang-Han Cao[c]

[a] Department of Physics, University of Ottawa, Ottawa, Ontario K1N 6N5, Canada
[b] Department of Physics, Majmaah University, P.O. Box 1712, Zulfi, Saudi Arabia
[c] Department of Physics, Zhejiang University, Hangzhou 310027, China

ARTICLE INFO

Keywords:
Spin-density-wave antiferromagnetism
Superconductivity

ABSTRACT

The findings of a ^{57}Fe and ^{151}Eu Mössbauer spectroscopy investigation between 1.8 and 299.5 K of $EuFeAs_2$ and the 14 K superconductor $EuFe_{0.97}Ni_{0.03}As_2$ are reported. In both compounds, the Fe sublattice orders in the antiferromagnetic spin-density-wave fashion with the Néel temperatures and Fe saturation magnetic moments of 106.2(1.9) K, 0.78(1)μ_B and 56.6(2.2) K, 0.47(1)μ_B, respectively. The Néel temperatures and the saturation hyperfine magnetic fields of the antiferromagnetically ordered Eu sublattice in both compounds are 44.4(5) K, 294.2(7) kOe and 43.5(1) K, 290.5(1) kOe, respectively. The 3% substitution of Fe by Ni in $EuFeAs_2$ has a dramatic effect on the magnetism of the Fe sublattice and virtually no effect on the magnetism of the Eu sublattice. The presence of Fe and Eu magnetic order in $EuFe_{0.97}Ni_{0.03}As_2$ is direct proof of the coexistence of superconductivity and magnetism. The increase of the magnitude of the main component of the electric field gradient tensor, at both Fe and Eu sites, with decreasing temperature is explained by a $T^{3/2}$ power-law relation. The Debye temperatures of $EuFeAs_2$, $EuFe_{0.97}Ni_{0.03}As_2$, and the $FeAs_2$ impurity phase are 355(18), 428(14), and 594(25) K, respectively.

1. Introduction

Recently, a new Eu-containing iron-pnictide compound $EuFeAs_2$ has been discovered [1]. The crystal structure of this compound is similar to that of the 112-type iron-pnictide (Ca,*R*) $FeAs_2$ (*R* = rare earth) superconductors. It consists of two Eu planes, Fe_2As_2 layers, and As_2-zigzag chain layers [2,3]. There is some discrepancy regarding the space group in which the $EuFeAs_2$ compound crystallizes. The monoclinic space group $P2_1/m$ was used in Refs. [1,4], and the orthorhombic space group *Imm*2 was employed in Ref. [3].

The two anomalies in the temperature dependence of the normalized resistivity of $EuFeAs_2$ at about 110 and 40 K were attributed to the probable antiferromagnetic spin-density-wave (SDW) transition of the Fe^{2+} ions, or the structural transition, and to the antiferromagnetic transition of the Eu^{2+} ions, respectively [1]. The antiferromagnetic transition at 41 K was also noticed in the temperature dependence of the magnetic susceptibility [1]. Similar anomalies (at about 100 and 40 K) were found in the resistivity data in Ref. [4]. However, a much more complex set of possible magnetic transitions was suggested based on the interpretation of the magnetic susceptibility and specific heat data [4].

It has been demonstrated recently that a small substitution of Fe by Ni in $EuFeAs_2$ induces superconductivity in $EuFe_{1-x}Ni_xAs_2$ with $x = 0.03$, 0.04, and 0.07 [4,5]. The critical temperature T_c for these three superconductors is 13.8, 17.5–18.2, and 13.7 K, respectively [4,5]. For the $x = 0.04$ superconductor, no antiferromagnetic SDW order of the Fe sublattice was observed, and the Eu sublattice was found to order antiferromagnetically below 38.5 K, followed by a putative spin-glass freezing at 15.5 K and a possible Eu-spin canting at 6.2 K [4]. What is remarkable about these new $EuFe_{1-x}Ni_xAs_2$ superconductors is the apparent coexistence of magnetism and superconductivity.

The Mössbauer spectroscopy technique proved to be a useful tool to study the possibility of incommensurate SDW order in a given compound. Its usefulness results from the fact that incommensurability leads to the complex shape of the Mössbauer spectra [6–9]. In this paper, we employ ^{57}Fe and ^{151}Eu Mössbauer spectroscopy to identify the nature of the Fe and Eu antiferromagnetic ordering in the non-superconducting $EuFeAs_2$ and the superconducting $EuFe_{0.97}Ni_{0.03}As_2$. We

* Corresponding author.
E-mail address: stadnik@uottawa.ca (Z.M. Stadnik).

https://doi.org/10.1016/j.jmmm.2020.166603
Received 2 January 2020; Received in revised form 8 February 2020; Accepted 9 February 2020
Available online 14 February 2020

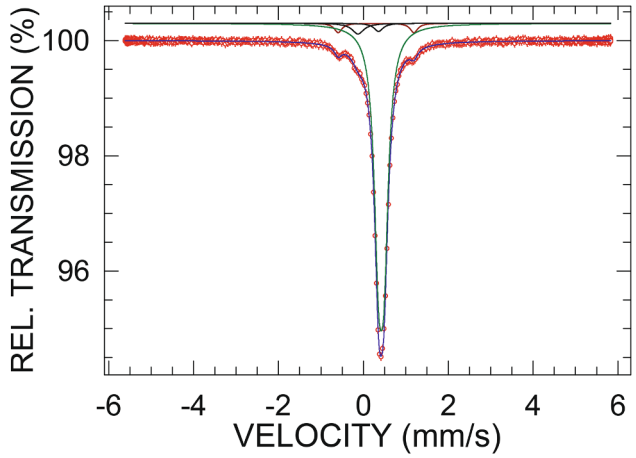

Fig. 1. High-statistics, ^{57}Fe Mössbauer spectrum of $EuFeAs_2$ at 299.8 K measured over a broad velocity range and fitted (solid blue line) with a large spectral area quadrupole doublet (solid dark green line) due to $EuFeAs_2$, a small spectral area quadrupole doublet (solid dark red line) originating from the $FeAs_2$ impurity phase, and two small spectral area single lines (solid black lines) which simulate the spectrum due to the presence of a tiny amount of Fe in the two Al foils of the absorber and in the two cryostat mylar windows, as described in the text. The zero-velocity origin is relative to α-Fe at room temperature.

show that both in $EuFeAs_2$ and $EuFe_{0.97}Ni_{0.03}As_2$, the Fe sublattice orders in the incommensurate SDW fashion, and with the magnetic parameters of the latter significantly smaller than those of the former. The Eu sublattice is shown to be also magnetically ordered in both compounds, but with the magnetic parameters that are practically the same.

2. Experimental methods

The polycrystalline samples of $EuFeAs_2$ and $EuFe_{0.97}Ni_{0.03}As_2$ used in this study were synthesized using a standard solid-state reaction method [4]. The powder X-ray diffraction spectra showed [4,5] that the $EuFeAs_2$ specimen contains a small amount of $FeAs_2$ impurity and the $EuFe_{0.97}Ni_{0.03}As_2$ specimen is impurity free.

The methodology of the ^{57}Fe and ^{151}Eu Mössbauer spectroscopy [10] measurements used here is the same as that described in Ref. [11]. The ^{57}Fe and ^{151}Eu Mössbauer spectra measured at temperatures below the Néel temperature T_N were analyzed using a first-order perturbation treatment [10] because the magnetic dipole interaction is much larger than the electric quadrupole interaction in the compounds studied.

The dc magnetic susceptibility was measured using a magnetic property measurement system (MPMS-5, Quantum Design). A standard four-electrode method was used to measure electrical resistivity.

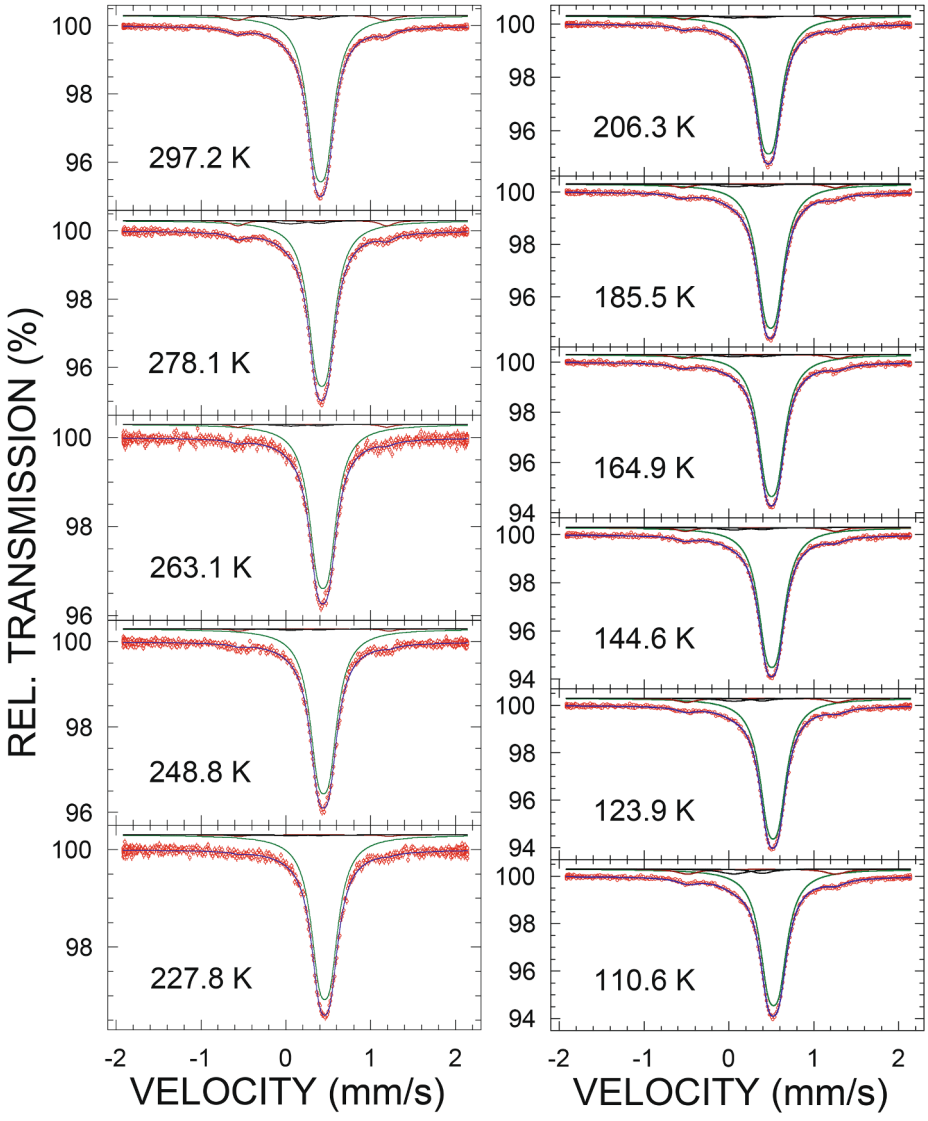

Fig. 2. ^{57}Fe Mössbauer spectra of $EuFeAs_2$ at temperatures above T_N of the Fe sublattice fitted in the same way as the spectrum in Fig. 1. The zero-velocity origin is relative to α-Fe at room temperature.

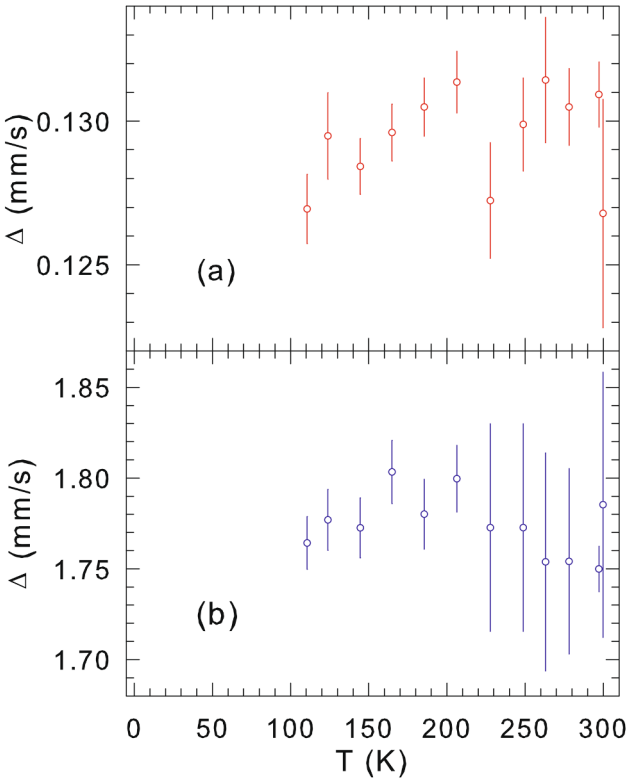

Fig. 3. Temperature dependence of the ^{57}Fe quadrupole splitting Δ of $EuFeAs_2$ (a) and $FeAs_2$ (b).

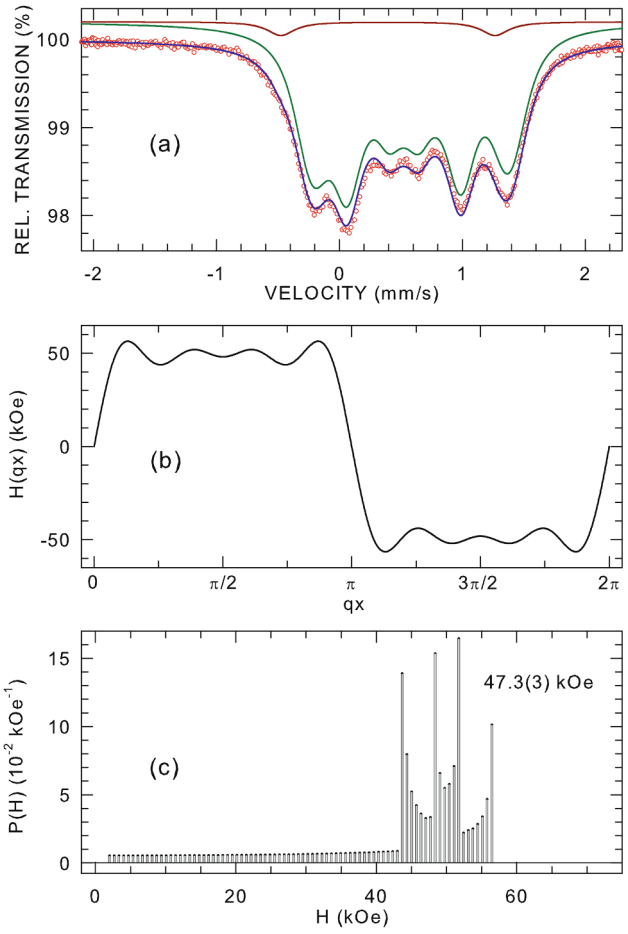

Fig. 4. (a) ^{57}Fe Mössbauer spectrum of $EuFeAs_2$ at 47.7 K fitted (solid blue line) with an incommensurate modulation of the hyperfine magnetic field pattern (solid dark green line) due to $EuFeAs_2$ and a quadrupole doublet (solid dark red line) originating from the $FeAs_2$ impurity phase, as described in the text. The zero-velocity origin is relative to α-Fe at room temperature. (b) Resulting shape of the SDW. (c) Resulting hyperfine magnetic field distribution labeled with the corresponding root-mean-square value of the hyperfine magnetic field. (For interpretation of the references to colour in this figure legend, the reader is referred to the web version of this article.)

3. Experimental results and discussion

3.1. $EuFeAs_2$ compound

The high-statistics, room-temperature ^{57}Fe Mössbauer spectrum of $EuFeAs_2$ was measured over a broad velocity range (Fig. 1) to check whether the sample studied contains any magnetically-ordered, Fe-containing impurity phase. The absence of any Zeeman pattern in the spectrum proves that such impurity is not present in the sample. The spectrum is the superposition of a quadrupole doublet (with a very small quadrupole splitting $\Delta = \frac{1}{2}eQ|V_{zz}|\sqrt{1+\eta^2/3}$, where the symbols e, Q, V_{zz}, and η have their usual meaning [10,11]) originating from the main phase, a quadrupole doublet (with a very large Δ) due to the $FeAs_2$ impurity [12], and two single lines (at ~ − 0.24 and ~0.25 mm/s) which simulate the spectrum of a tiny amount of Fe present in the two Al foils of the absorber and the two cryostat mylar windows.

Fig. 2 displays the ^{57}Fe Mössbauer spectra of $EuFeAs_2$ measured in the paramagnetic temperature region, that is, above T_N of the Fe sublattice, and over a narrow velocity range. They can be fitted well with three components, similarly as the spectrum in Fig. 1.

The temperature dependence of Δ of $EuFeAs_2$ obtained from the fits of the spectra in Figs. 1,2 is shown in Fig. 3(a). Within the statistical error, it appears to be temperature independent. A similar conclusion is arrived at for the temperature dependence of Δ of the $FeAs_2$ impurity [Fig. 3(b)].

The ^{57}Fe Mössbauer spectrum of $EuFeAs_2$ at 47.7 K, that is, much below T_N of the Fe sublattice, is shown in Fig. 4(a). It is in the form of an immensely broadened, asymmetric, six-line Zeeman pattern that differs significantly from the spectrum expected for an antiferromagnet with Fe atoms occupying one crystallographic site (sharp, symmetric, six-line Zeeman pattern) [10]. The significant line broadening must arise from the presence of wide distribution, $P(H)$, of hyperfine magnetic fields H. There are two possible sources of such a wide distribution of H [9]. First, it can result from significant structural disorder present in $EuFeAs_2$. Second, it may also arise from the incommensurate modulation of the antiferromagnetic structure (the incommensurate SDW). As there is no dopant-induced (substituting Fe with another metal) structural disorder in $EuFeAs_2$, one can assert that the complex shape of the spectrum in Fig. 4(a) originates from the incommensurate antiferromagnetic SDW.

To generate Mössbauer spectra caused by the incommensurate SDW, we follow the procedure described in detail in Ref. [7]. Briefly, the amplitude of the hyperfine magnetic field H due to the SDW along the x-direction that is parallel to the wave vector **q** is expressed as a series of odd harmonics [8]

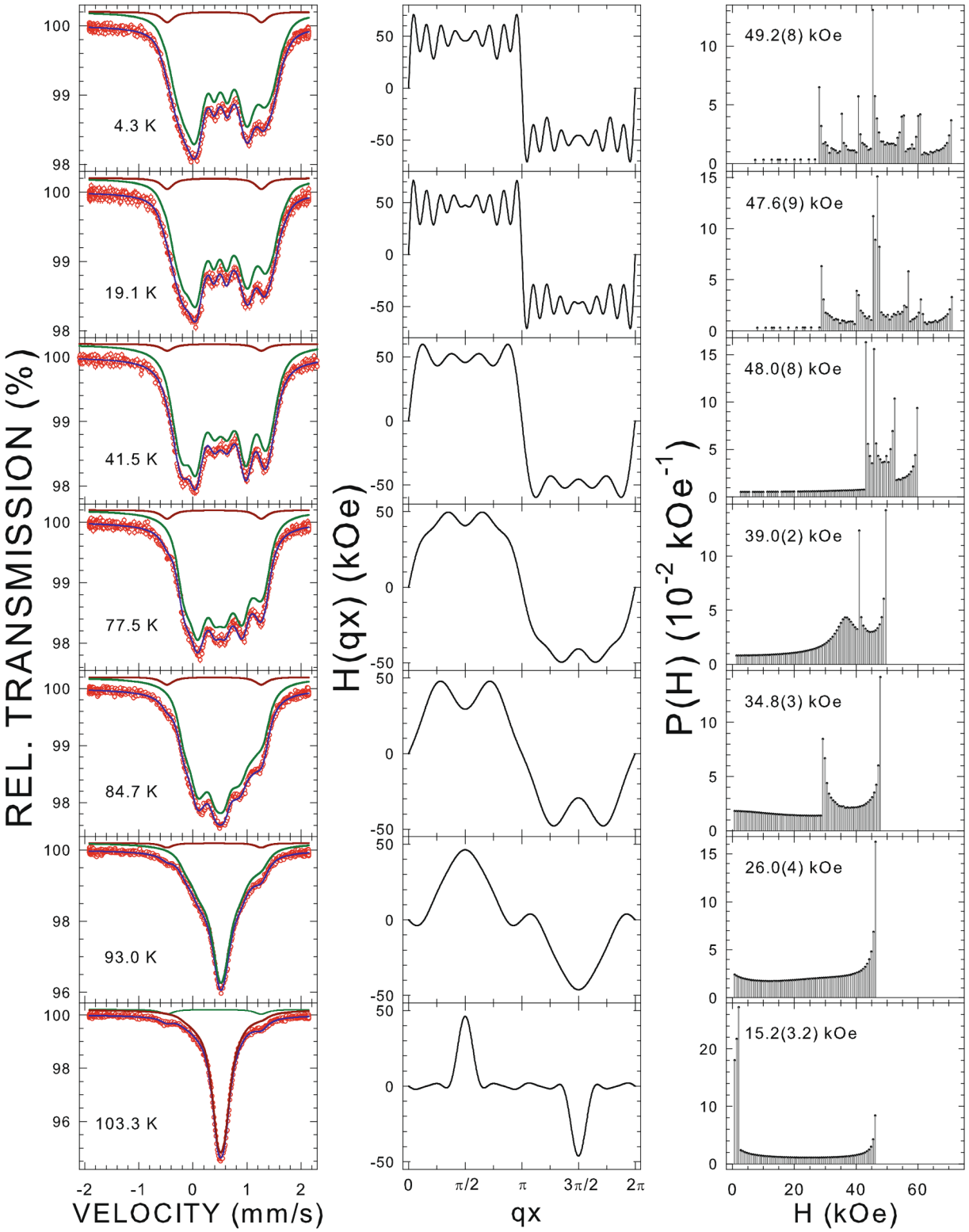

Fig. 5. ^{57}Fe Mössbauer spectra of $EuFeAs_2$ at the indicated temperatures fitted (solid blue line) with an incommensurate modulation of the hyperfine magnetic field pattern (solid dark green line) due to $EuFeAs_2$ and a quadrupole doublet (solid dark red line) arising from the $FeAs_2$ impurity phase (left panel), corresponding shapes of the SDW (middle panel), and resulting hyperfine magnetic field distributions labeled with the corresponding root-mean-square value of the hyperfine magnetic field (right panel). (For interpretation of the references to colour in this figure legend, the reader is referred to the web version of this article.)

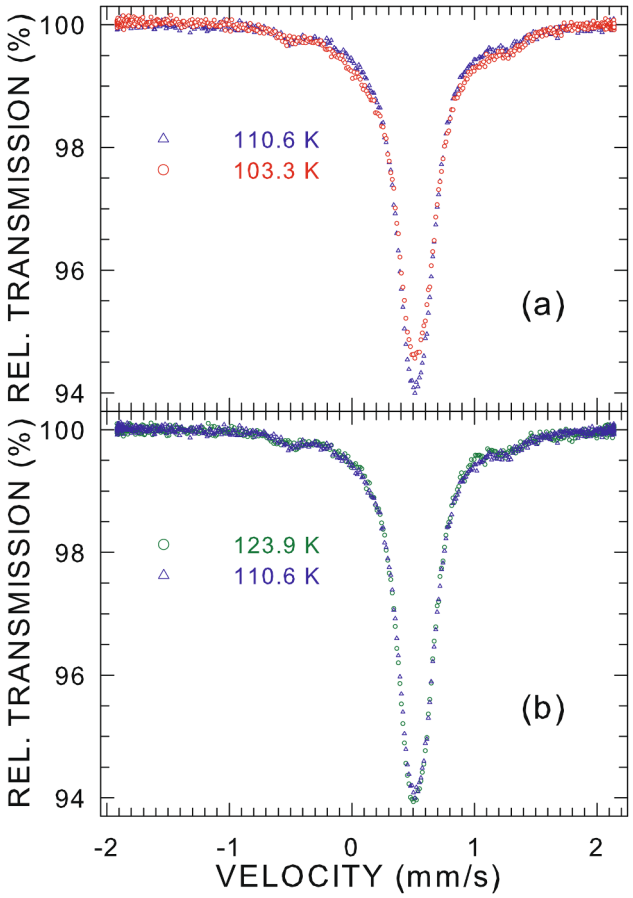

Fig. 6. Comparison of the ^{57}Fe Mössbauer spectra of $EuFeAs_2$ at 110.6 and 103.3 K (a) and at 123.9 and 110.6 K (b). The zero-velocity origin is relative to α-Fe at room temperature.

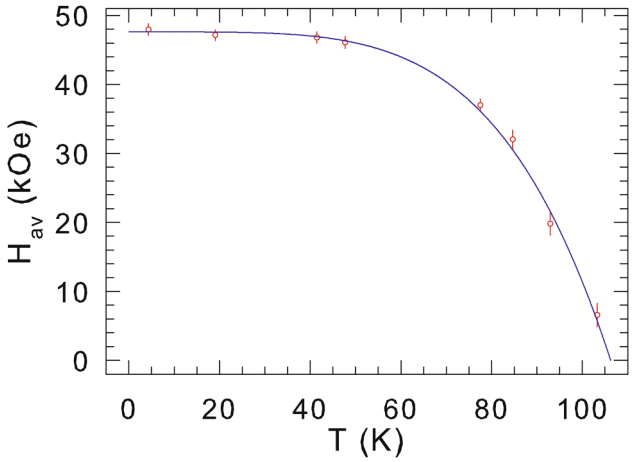

Fig. 7. Temperature dependence of H_{av} at ^{57}Fe nuclei derived from the distributions $P(H)$ in Figs. 4 and 5. The solid line is the power-law fit.

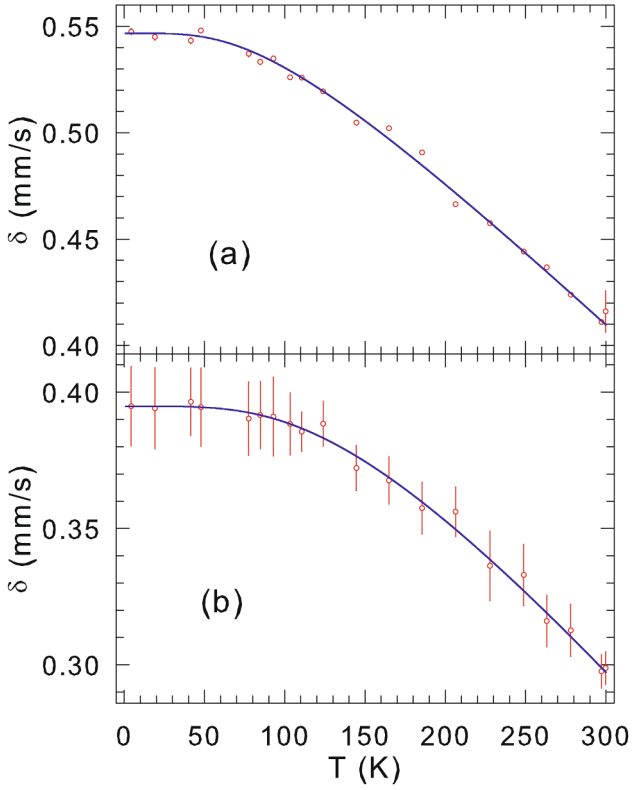

Fig. 8. Temperature dependence of the ^{57}Fe center shift δ of $EuFeAs_2$ (a) and $FeAs_2$ (b). The solid lines are the fits to Eq. (2), as explained in the text.

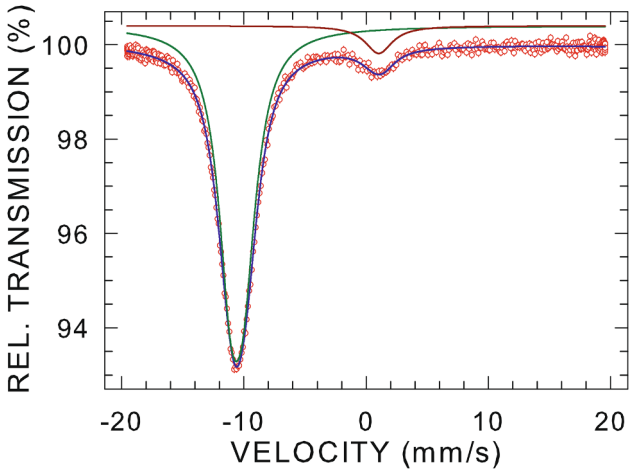

Fig. 9. ^{151}Eu Mössbauer spectrum of $EuFeAs_2$ at 298.2 K fitted (solid blue line) with a large spectral area quadrupole pattern due to $EuFeAs_2$ (solid dark green line) and a small spectral area singlet originating from an impurity phase (solid dark red line), as described in the text. The zero-velocity origin is relative to the source. (For interpretation of the references to colour in this figure legend, the reader is referred to the web version of this article.)

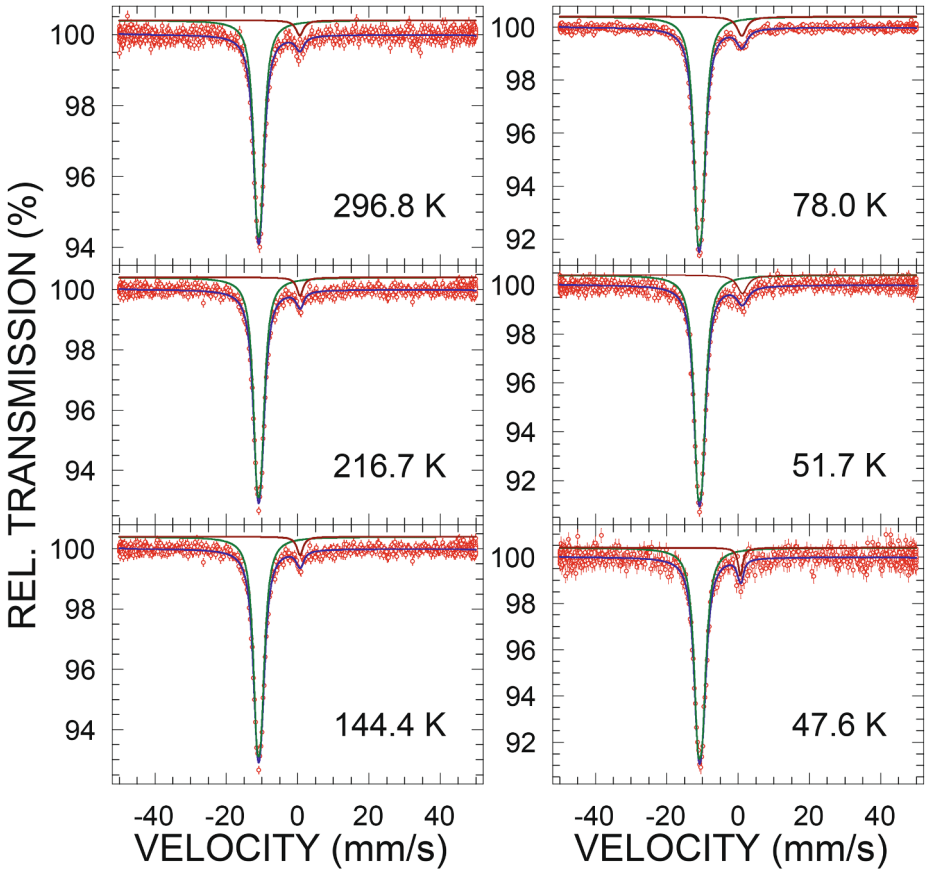

Fig. 10. ^{151}Eu Mössbauer spectra of $EuFeAs_2$ at the indicated temperature fitted in the same way as the spectrum in Fig. 9. The zero-velocity origin is relative to the source.

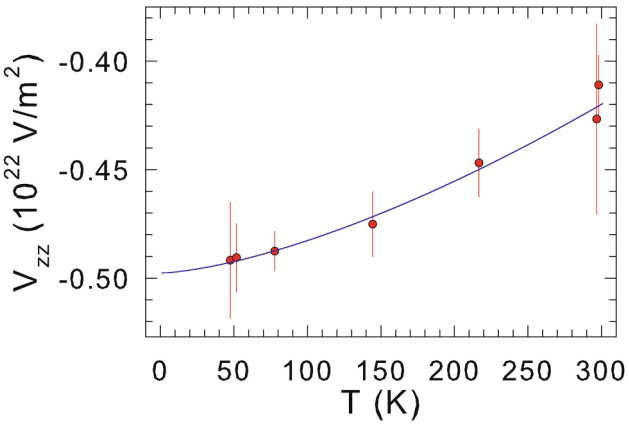

Fig. 11. Temperature dependence of the principal component of the electric field gradient tensor V_{zz} at ^{151}Eu nuclei derived from the fits of the spectra in Figs. 9 and 10. The solid line is the fit to Eq. (4), as explained in the text.

$$H(qx) = \sum_{i=1}^{n} h_{2i-1}\sin[(2i-1)qx], \quad (1)$$

where h_{2i-1} denotes the amplitude of the (2i-1) th harmonic and n is the maximum number of harmonics. One fits then an experimental Mössbauer spectrum with a finite number of six-line Zeeman patterns corresponding to H values that are calculated from Eq. (1) for individual qx values from the range $\langle 0, 2\pi\rangle$. The amplitudes h_{2i-1} obtained from the fit are used to calculate the resulting distribution $P(H)$. They can also be used to calculate the root-mean-square value of H, $H_{\rm rms} = \sqrt{\frac{1}{2}\sum_{i=1}^{n} h_{2i-1}^2}$, which is proportional to the magnetic moment $\mu_{\rm Fe}$ carried by the Fe atoms. The knowledge of the $P(H)$ distribution allows one to calculate the average hyperfine magnetic field $H_{\rm av} \equiv < |H| >$.

The ^{57}Fe Mössbauer spectrum in Fig. 4(a) was fitted with two components. The first, large spectral area, SDW component originates from $EuFeAs_2$. The second, small spectral area, quadrupole doublet component arises from the $FeAs_2$ impurity. Because the spectrum of a tiny amount of Fe present in the two Al foils of the absorber and the two cryostat mylar windows in the form of two single lines (Figs. 1 and 2) completely overlaps with the central portion of the experimental spectrum in Fig. 4(a), it was not possible to include it in the fit. A good fit of the Mössbauer spectrum in Fig. 4(a) was obtained with $n = 4$ harmonics. The resulting shape of the SDW and corresponding distribution $P(H)$ are shown in Figs. 4(b) and 4(c), respectively. The parameters obtained from the fit are: the centre shift [10] $\delta = 0.552(1)$ mm/s, the quadrupole shift [10] $\varepsilon = 0.027(1)$ mm/s, $H_{\rm max} = 56.5(1)$ kOe, $H_{\rm av} = 46.1(1)$ kOe, and $H_{\rm rms} = 47.3(3)$ kOe.

The ^{57}Fe Mössbauer spectra of $EuFeAs_2$ at other temperatures below T_N (Fig. 5) were fitted in like manner as the 47.7 K spectrum (Fig. 4).

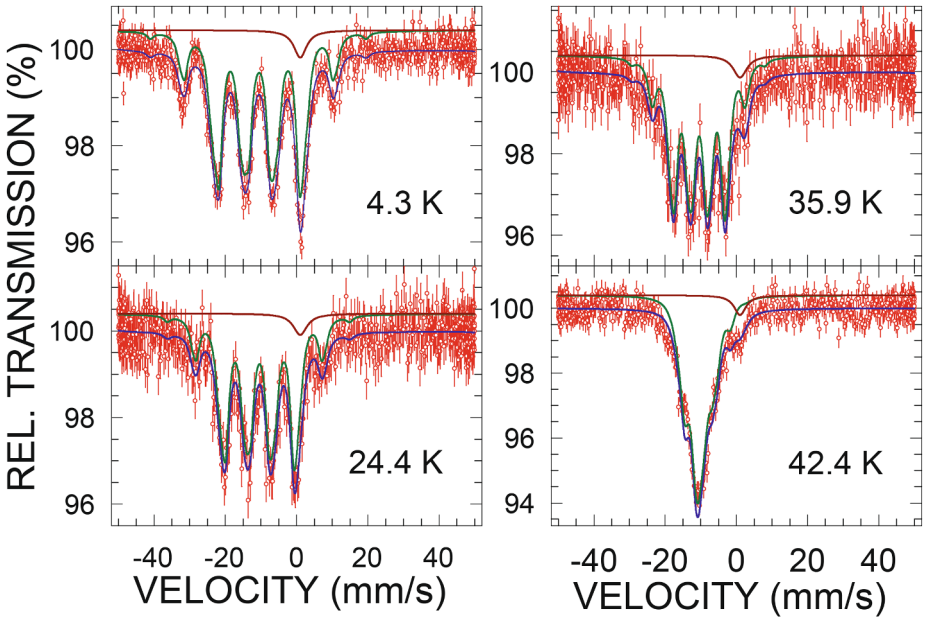

Fig. 12. ^{151}Eu Mössbauer spectrum of $EuFeAs_2$ at the indicated temperatures fitted (solid blue lines) with a large spectral area Zeeman pattern due to $EuFeAs_2$ (solid dark green lines) and a small spectral area single line originating from an impurity phase (solid dark red lines), as described in the text. The zero-velocity origin is relative to the source. (For interpretation of the references to colour in this figure legend, the reader is referred to the web version of this article.)

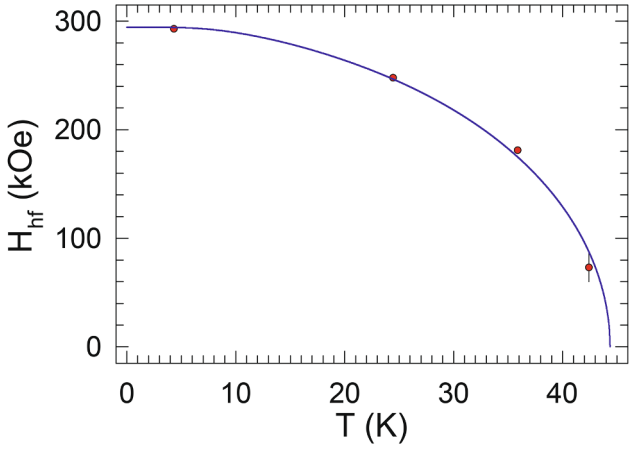

Fig. 13. Temperature dependence of the hyperfine magnetic field H_{hf} at ^{151}Eu nuclei obtained from the fits of the spectra in Fig. 12. The solid line is the fit to Eq. (5), as explained in the text.

One observes that the shape of the SDW (Figs. 4 and 5) changes from the nearly rectangular one at low temperatures to the nearly triangular one at high temperatures (close to T_N).

One could wonder why the spectrum at 103.6 K (Fig. 5), which visually looks the same as the paramagnetic spectrum at 110.6 K (Fig. 2), is fitted with a SDW component. A comparison of these two spectra [Fig. 6(a)] reveals two differences. The width and the relative transmission of the 103.3 K spectrum are larger than the corresponding width and the relative transmission of the 110.6 K spectrum. Such differences are not observed between the neighboring 123.9 and 110.6 K paramagnetic spectra [Fig. 6(b)]. This proves that the 103.3 K spectrum must be due to a magnetically ordered component. Fig. 6(a) also indicates that T_N of the Fe sublattice must be between 103.3 and

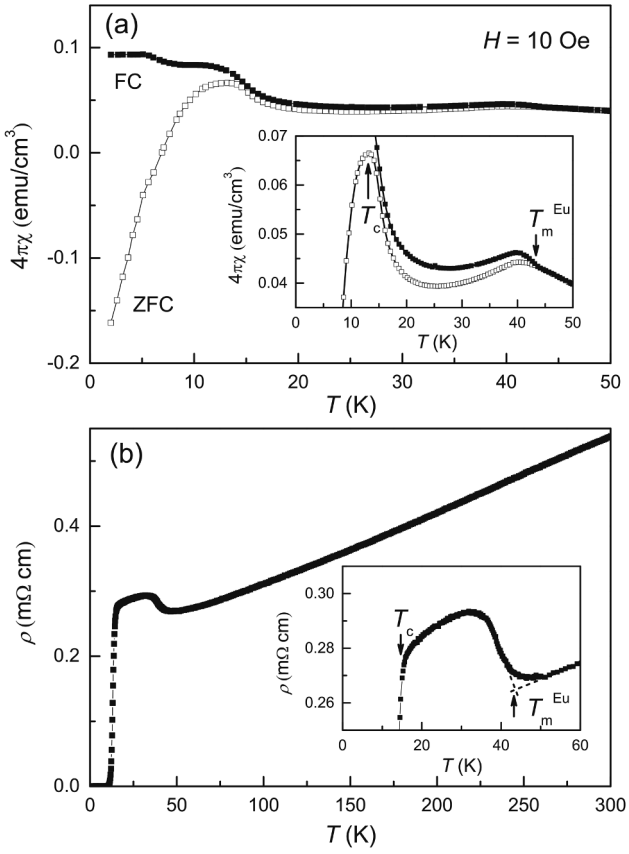

Fig. 14. Temperature dependence of the ZFC and FC magnetic susceptibility (a) and the electrical resistivity (b) of $EuFe_{0.97}Ni_{0.03}As_2$. The insets show the ordinate magnifications around the T_c and T_m^{Eu} temperatures.

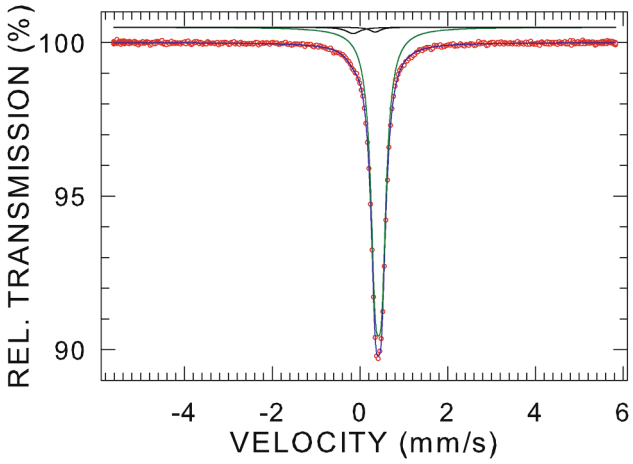

Fig. 15. High-statistics, ^{57}Fe Mössbauer spectrum of $EuFe_{0.97}Ni_{0.03}As_2$ at 298.9 K measured over a broad velocity range and fitted (solid blue line) with a large spectral area quadrupole doublet (solid dark green line) due to $EuFe_{0.97}Ni_{0.03}As_2$ and two small spectral area single lines (solid black lines) which simulate the spectrum due to the presence of a tiny amount of Fe in the two Al foils of the absorber and in the two cryostat mylar windows, as described in the text. The zero-velocity origin is relative to α-Fe at room temperature. (For interpretation of the references to colour in this figure legend, the reader is referred to the web version of this article.)

110.6 K.

The temperature dependence of the H_{av} values, that were calculated from the distributions $P(H)$ shown in Figs. 4 and 5, is displayed in Fig. 7. The expected increase of H_{av} with decreasing temperature is observed. Fitting the H_{av} data to the power law over the limited temperature range yields the value of H_{av} at 0 K, $H_{av}(0) = 47.6(9)$ kOe, and $T_N = 106.2(1.9)$ K. The value of T_N found here is comparable to the value of ~110 K estimated from the resistivity and magnetic susceptibility data [1,4].

By extrapolating the $H_{rms}(T)$ data (Fig. 5) to 0 K, the value of H_{rms} at 0 K, $H_{rms}(0)$, was found to be 49.4(4) kOe. The hyperfine magnetic field is approximately proportional to the Fe magnetic moment through the relation $H = a\mu_{Fe}$. The value of the proportionality constant a depends on a compound [10,13]. We used $a = 63$ kOe/μ_B (Ref. [9]) to convert $H_{rms}(0)$ to $\mu_{Fe}(0)$. Thus, $H_{rms}(0) = 49.4(4)$ kOe corresponds to $\mu_{Fe}(0) = 0.78(1)\mu_B$.

The temperature dependence of the centre shift [10] $\delta(T)$ of $EuFeAs_2$, obtained from the fits of the spectra in Figs. 1, 2, 4, and 5, is shown in Fig. 8(a). $\delta(T)$ is the sum of two physical quantities [10]

$$\delta(T) = \delta_0 + \delta_{SOD}(T). \tag{2}$$

The first quantity δ_0 is the intrinsic isomer shift. The second quantity $\delta_{SOD}(T)$ is the second-order Doppler (SOD) shift. The latter can be expressed in terms of the Debye temperature, Θ_D, as

$$\delta_{SOD}(T) = -\frac{9}{2}\frac{k_B T}{Mc}\left(\frac{T}{\Theta_D}\right)^3 \int_0^{\Theta_D/T} \frac{x^3 dx}{e^x - 1}. \tag{3}$$

Here the symbols k_B, M, and c have their usual meaning [10]. The fit of the experimental data in Fig. 8(a) to Eq. (2) yields $\delta_0 = 0.547(2)$ mm/s and $\Theta_D = 355(18)$ K.

A similar fit of the $\delta(T)$ data for the $FeAs_2$ impurity [Fig. 8(b)] gives $\delta_0 = 0.387(3)$ mm/s and $\Theta_D = 594(25)$ K.

The room-temperature ^{151}Eu Mössbauer spectrum of $EuFeAs_2$ measured over the velocity range ∓20 mm/s is shown in Fig. 9. The component with a large spectral area arises from Eu atoms in $EuFeAs_2$ and appears as an unresolved 12-line quadrupole pattern [10,14]. The component with a small spectral area derives from Eu^{3+} ions in an unknown foreign phase and comes out as a single line. The following parameters are obtained from the fit of the spectrum in Fig. 9: the isomer shift [relative to the $^{151}Sm(SmF_3)$ source] $\delta = -10.56(1)$ mm/s, $V_{zz} = -0.411(14) \times 10^{22}$ V/m^2, and $\eta = 0.74(9)$. The value of δ proves that Eu in $EuFeAs_2$ is in the divalent state [10,14].

The ^{151}Eu Mössbauer spectra of $EuFeAs_2$ measured over the velocity range ∓50 mm/s at other temperatures above T_N of the Eu sublattice are shown in Fig. 10. They are fitted analogously as the spectrum in Fig. 9.

Fig. 11 displays the temperature dependence of V_{zz} derived from the fits of the spectra in Figs. 9 and 10. One notices an increase of the magnitude of V_{zz} with decreasing temperature. The empirical $T^{3/2}$ power-law relation

$$V_{zz}(T) = V_{zz}(0)(1 - BT^{3/2}) \tag{4}$$

fits well the $V_{zz}(T)$ data. Here $V_{zz}(0)$ is the value of V_{zz} at 0 K and B is a constant. The fit of the $V_{zz}(T)$ data (Fig. 11) to Eq. (4) gives $V_{zz}(0) = -0.498(5) \times 10^{22}$ V/m^2 and $B = 3.01(18) \times 10^{-5}$ K$^{-3/2}$. It should be noted here that a similar $T^{3/2}$ dependence of $V_{zz}(T)$ has been observed in other Eu-containing compounds, such as $EuPdGe_3$ [15], $CsEuFe_4As_4$ [11], and $RbEuFe_4As_4$ [16]. Such a $T^{3/2}$ dependence of V_{zz} at ^{57}Fe nuclei has also been observed in hundreds of Fe-containing metallic compounds [16]. Its origin still remains elusive [17].

Fig. 12 displays the ^{151}Eu Mössbauer spectra of $EuFeAs_2$ measured at temperatures below T_N of the Eu sublattice. They are fitted with a Zeeman pattern component of a large spectral area which is due to $EuFeAs_2$, and a single line component of a small spectral area which arises from an unknown Eu^{3+}-containing impurity phase.

The temperature dependence of the hyperfine magnetic field H_{hf} obtained from the fits to the Mössbauer spectra in Fig. 12 is shown in Fig. 13. Within the molecular field model, it is assumed that H_{hf} in a magnetically ordered compound is proportional to the sublattice magnetization. Thus, the $H_{hf}(T)$ dependence can be written as

$$H_{hf}(T) = H_{hf}(0)B_J(x). \tag{5}$$

Here $H_{hf}(0)$ represents the saturation hyperfine magnetic field (the field at 0 K), $B_J(x)$ is the Brllouin function [18]

$$B_J(x) = \frac{2J+1}{2J}\coth\left(\frac{2J+1}{2J}x\right) - \frac{1}{2J}\coth\left(\frac{x}{2J}\right) \tag{6}$$

and

$$x = \frac{3J}{J+1}\frac{H_{hf}(T)}{H_{hf}(0)}\frac{T_N}{T}. \tag{7}$$

The fit of the $H_{hf}(T)$ data (Fig. 13) to Eq. (5) with $J = S = 7/2$ gives $H_{hf}(0) = 294.2(7)$ kOe and $T_N = 44.4(5)$ K. For ^{151}Eu Mössbauer spectroscopy [14,19], there is no simple relation between $H_{hf}(0)$ and the saturation magnetic moment of the Eu atoms, $\mu_{Eu}(0)$. Consequently, one thus cannot determine reliably $\mu_{Eu}(0)$ from $H_{hf}(0)$.

The ^{57}Fe and ^{151}Eu Mössbauer data presented above show that in $EuFeAs_2$, the Fe sublattice orders in the incommensurate SDW fashion with $T_N = 106.2(1.9)$ K and $\mu_{Fe}(0) = 0.78(1)\mu_B$, whereas the Eu sublattice is magnetically ordered below $T_N = 44.4(5)$ K and with $H_{hf}(0) = 294.2(7)$ kOe.

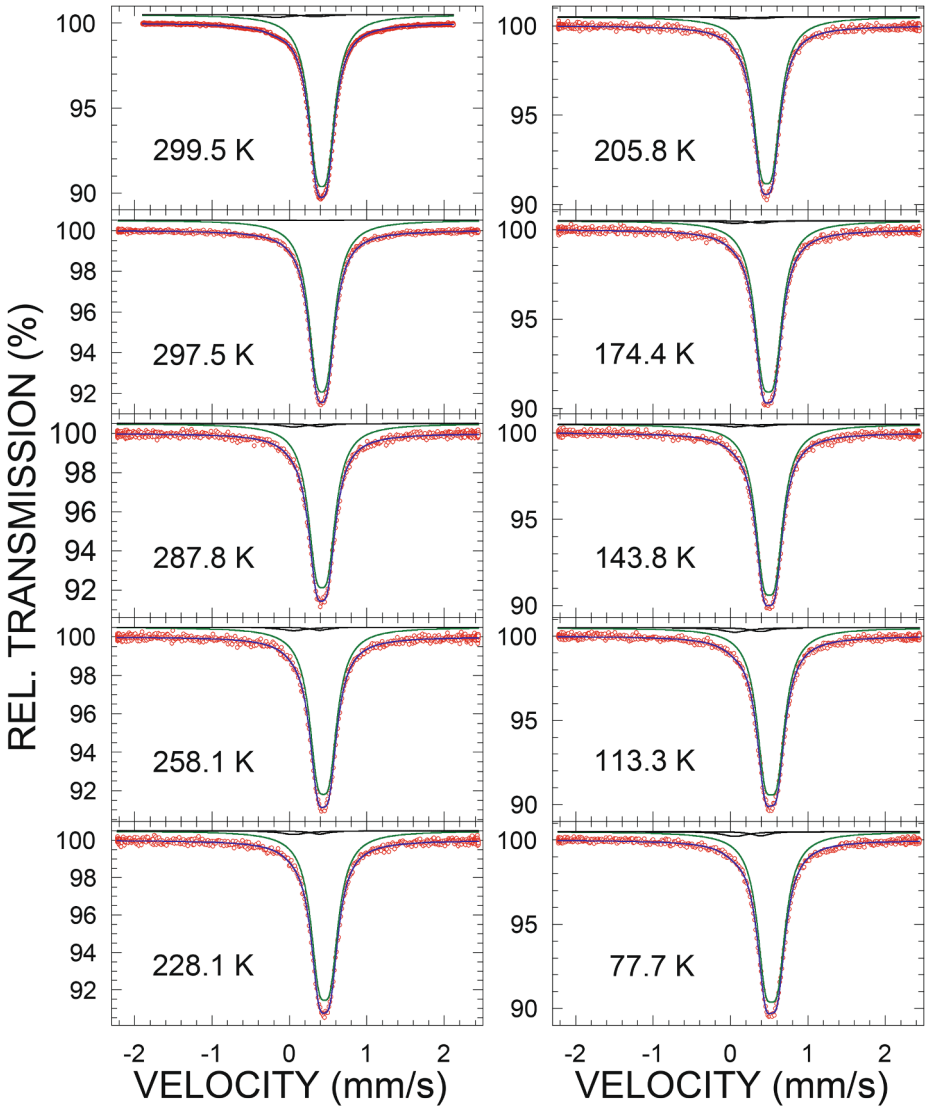

Fig. 16. ^{57}Fe Mössbauer spectra of $EuFe_{0.97}Ni_{0.03}As_2$ at temperatures above T_N of the Fe sublattice fitted in the same way as the spectrum in Fig. 15. The zero-velocity origin is relative to α-Fe at room temperature.

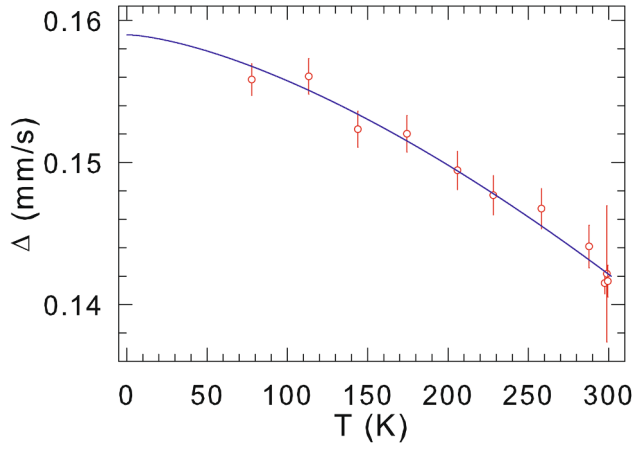

Fig. 17. Temperature dependence of the ^{57}Fe quadrupole splitting Δ of $EuFe_{0.97}Ni_{0.03}As_2$ obtained from the fits of the spectra in Figs. 15 and 16. The solid line is the fit to the $T^{3/2}$ power-law relation, as explained in the text.

3.2. *$EuFe_{0.97}Ni_{0.03}As_2$ superconductor*

The temperature dependence of the zero-field-cooled (ZFC) and field-cooled (FC) magnetic susceptibility χ of $EuFe_{0.97}Ni_{0.03}As_2$ measured in an applied field of 10 Oe is shown in Fig. 14(a). The bifurcation of the ZFC and FC χ data occurs at about 14 K. The diamagnetic ZFC χ decreases with decreasing temperature and this proves that the compound studied is a superconductor. The anomaly of the χ data at the temperature T_m^{Eu} of about 43 K may be possibly associated with the magnetic transition of the Eu sublattice. The temperature dependence of the resistivity ρ of $EuFe_{0.97}Ni_{0.03}As_2$ [Fig. 14(b)] indicates that $T_c = 13.8$ K. The anomaly at T_m^{Eu} probably results from the magnetic ordering of the Eu sublattice.

Fig. 15 shows the high-statistics, room-temperature ^{57}Fe Mössbauer spectrum of $EuFe_{0.97}Ni_{0.03}As_2$ measured over a large velocity range. The absence of any Zeeman pattern shows that the specimen studied is free of any Fe-containing magnetic impurity. In contrast to a similar spectrum of $EuFeAs_2$ (Fig. 1), no contribution originating from the

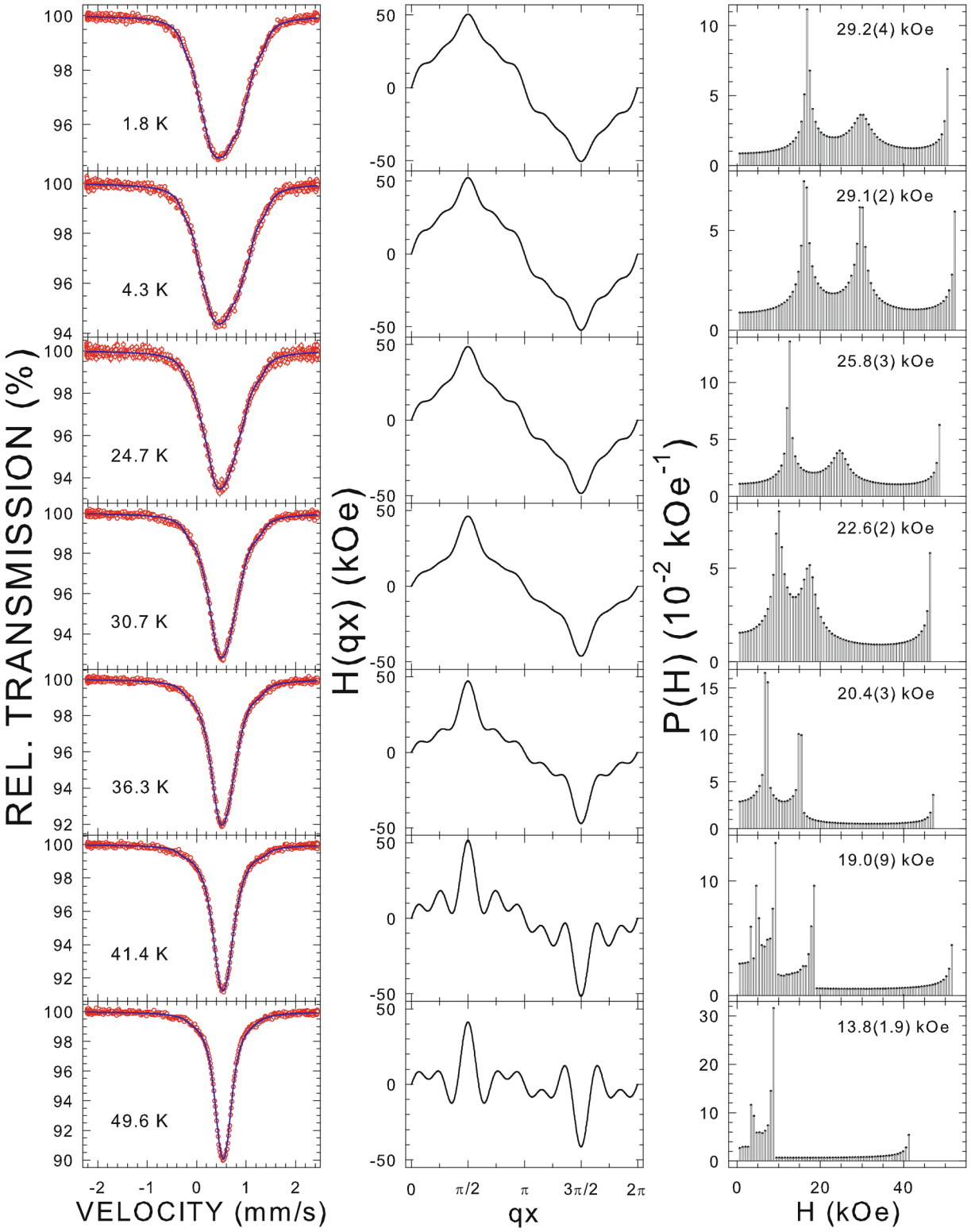

Fig. 18. ^{57}Fe Mössbauer spectra of $EuFe_{0.97}Ni_{0.03}As_2$ at the indicated temperatures fitted (solid blue line) with an incommensurate modulation of the hyperfine magnetic field pattern (left panel), corresponding shapes of the SDW (middle panel), and resulting hyperfine magnetic field distributions labeled with the corresponding root-mean-square value of the hyperfine magnetic field (right panel).

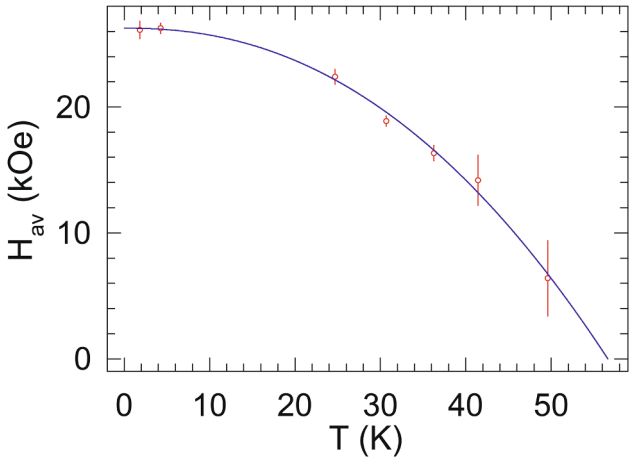

Fig. 19. Temperature dependence of H_{av} at ^{57}Fe nuclei obtained from the distributions $P(H)$ in Fig. 18. The solid line is the power-law fit.

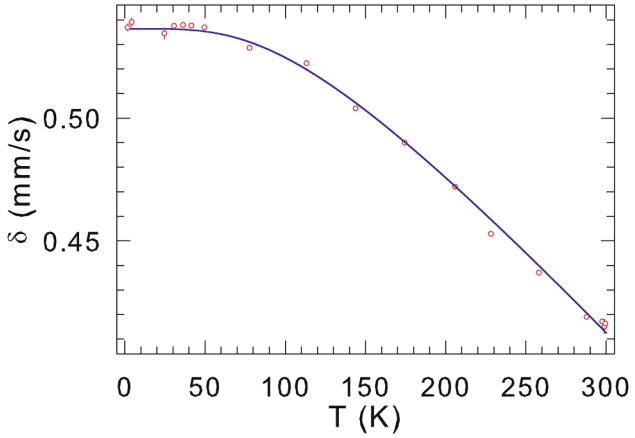

Fig. 20. Temperature dependence of the ^{57}Fe center shift δ of $EuFe_{0.97}Ni_{0.03}As_2$. The solid line is the fit to Eq. (2), as explained in the text.

$FeAs_2$ impurity can be detected (Fig. 15), in agreement with the X-ray diffraction results [4,5]. The only external contribution in the form of two single lines comes from a tiny amount of Fe present in the two Al foils of the absorber and the two cryostat mylar windows.

The ^{57}Fe Mössbauer spectra of $EuFe_{0.97}Ni_{0.03}As_2$ measured at temperatures above T_N of the Fe sublattice, and over a small velocity range, are shown in Fig. 16. They are fitted well with two components in the same way as the spectrum in Fig. 15.

Fig. 17 displays the temperature dependence of Δ of $EuFe_{0.97}Ni_{0.03}As_2$ derived from the fits of the spectra in Figs. 15,16. Analogously to the $V_{zz}(T)$ dependence in Fig. 11, one observes that Δ increases with decreasing temperature. The fit of the $\Delta(T)$ data to the same empirical $T^{3/2}$ power-law relation [(Eq. (4)], in which $V_{zz}(T)$ is substituted by $\Delta(T)$ and $V_{zz}(0)$ by $\Delta(0)$, yields $\Delta(0) = 0.1590(17)$ mm/s and $B = 20.4(2.6) \times 10^{-6}$ K$^{-3/2}$. The value of B determined here is close to that observed for other crystalline, quasicrystalline, and amorphous compounds [16].

The ^{57}Fe Mössbauer spectra of $EuFe_{0.97}Ni_{0.03}As_2$ at temperatures below T_N of the Fe sublattice are shown in Fig. 18. They were fitted with an incommensurate SDW pattern. No two-single line component, originating from a tiny amount of Fe present in the two Al foils of the absorber and the two cryostat mylar windows, could be included in the fit for the same reason as that given for the fits of the spectra in Figs. 4 and 5 (*vide supra*).

The values of H_{av} that were calculated from the distributions $P(H)$ in Fig. 18 are shown in Fig. 19. The fit of the H_{av} data to the power law (Fig. 19) gives $H_{av}(0) = 26.3(8)$ kOe and $T_N = 56.6(2.4)$ K. Extrapolating the $H_{rms}(T)$ data (Fig. 18) to 0 K gives $H_{rms}(0) = 29.5(4)$ kOe. This value of $H_{rms}(0)$ corresponds to $\mu_{Fe}(0) = 0.47(1)\mu_B$.

Implicit in the above analysis is the assumption that the hyperfine magnetic field at the ^{57}Fe nuclei in $EuFe_{0.97}Ni_{0.03}As_2$ is an intrinsic one, that is, it results from the non-zero magnetic moment carried by the Fe atoms. However, one should also consider the possibility that the Fe atoms carry no magnetic moment and that the observed hyperfine magnetic field is due only to the transferred hyperfine magnetic field, H_{tr} [20], from the magnetically ordered Eu sublattice (*vide infra*). Experimentally, the value of H_{tr} at 0 K in superconductors containing Fe and Eu atoms was found to be below 10 kOe [11,16,21]. The value of $H_{rms}(0)$ found here is significantly larger than 10 kOe. It, therefore, appears that the observed hyperfine magnetic field in $EuFe_{0.97}Ni_{0.03}As_2$ is due to the non-zero Fe magnetic moment rather than to the transferred hyperfine magnetic field.

Fig. 20 presents the temperature dependence of $\delta(T)$ derived from the fits of the spectra in Figs. 15,16,18. The fit of the $\delta(T)$ data to Eq. (2) yields $\delta_0 = 0.536(2)$ mm/s and $\Theta_D = 428(14)$ K.

The ^{151}Eu Mössbauer spectra of $EuFe_{0.97}Ni_{0.03}As_2$ measured at temperatures above T_N of the Eu sublattice are displayed in Fig. 21. They are fitted in like manner as the spectra in Fig. 10. The values of V_{zz} obtained from the fits of the spectra in Fig. 21 are plotted in Fig. 22. One observes that the magnitude of V_{zz} increases with decreasing temperature. The fit of the $V_{zz}(T)$ data (Fig. 22) to Eq. (4) yields $V_{zz}(0) = -0.448(5) \times 10^{22}$ V/m^2 and $B = 3.28(29) \times 10^{-5}$ K$^{-3/2}$.

Fig. 23 shows the ^{151}Eu Mössbauer spectra of $EuFe_{0.97}Ni_{0.03}As_2$ measured at temperatures below T_N of the Eu sublattice. They are fitted with a Zeeman pattern component of a large spectral area that derives from $EuFe_{0.97}Ni_{0.03}As_2$ and a single line component of a small spectral area that originates from a Eu^{3+}-containing an unknown impurity.

Fig. 24 displays the temperature dependence of H_{hf} determined from the fits to the Mössbauer spectra in Fig. 23. The fit of the $H_{hf}(T)$ dependence to Eq. (5) with $J = S = 7/2$ yields $H_{hf}(0) = 290.5(1)$ kOe and $T_N = 43.5(1)$ K.

The analysis of the ^{57}Fe and ^{151}Eu Mössbauer spectra of $EuFe_{0.97}Ni_{0.03}As_2$ presented above shows that, similarly as in $EuFeAs_2$, the Fe sublattice orders in the incommensurate SDW fashion, but with a significantly smaller values of $T_N = 56.6(2.4)$ K and of $\mu_{Fe}(0) = 0.47(1)\mu_B$. On the other hand, the Eu sublattice in $EuFe_{0.97}Ni_{0.03}As_2$ is magnetically ordered below marginally lower $T_N = 43.5(1)$ K and with slightly lower $H_{hf}(0) = 290.5(1)$ kOe as compared to the corresponding values for $EuFeAs_2$. One can thus conclude that a 3% substitution of Fe by Ni in $EuFeAs_2$ dramatically reduces the magnetism of the Fe sublattice, but has virtually no effect on the magnetism of the Eu sublattice. The presence of the Fe and Eu antiferromagnetic order in $EuFe_{0.97}Ni_{0.03}As_2$ proves that superconductivity and antiferromagnetism coexist in this compound.

4. Conclusions

We describe the results of ^{57}Fe and ^{151}Eu Mössbauer spectroscopy measurements in the temperature range 1.8–299.5 K of $EuFeAs_2$ and the 14 K the superconductor $EuFe_{0.97}Ni_{0.03}As_2$. We find that in both

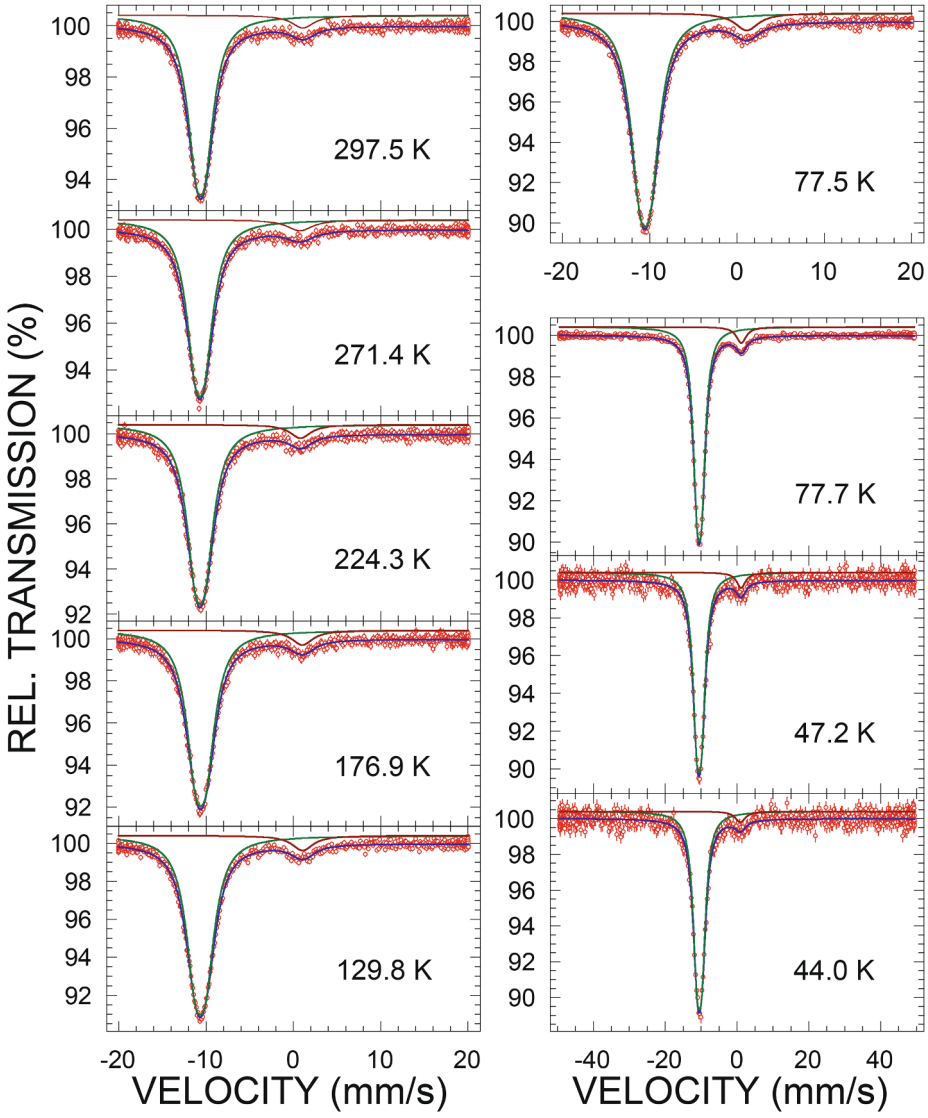

Fig. 21. ^{151}Eu Mössbauer spectra of $EuFe_{0.97}Ni_{0.03}As_2$ at the indicated temperature fitted in the same way as the spectra in Fig. 10. The zero-velocity origin is relative to the source.

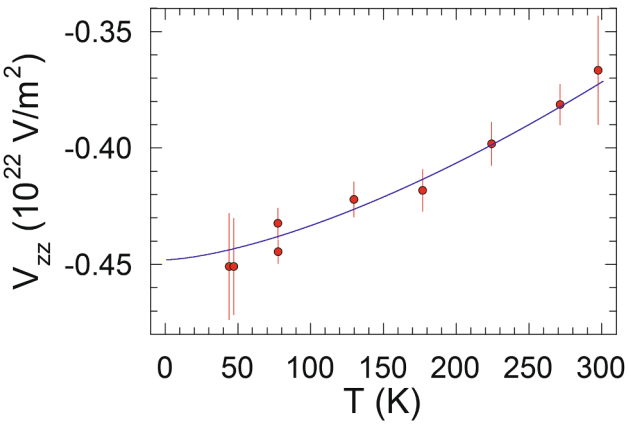

Fig. 22. Temperature dependence of the principal component of the electric field gradient tensor V_{zz} at ^{151}Eu nuclei determined from the fits of the spectra in Fig. 21. The solid line is the fit to Eq. (4), as explained in the text.

compounds the antiferromagnetic ordering of the Fe sublattice is of a spin-density-wave type with the Néel temperatures and Fe saturation magnetic moments of 106.2(1.9) K, $0.78(1)\mu_B$ and 56.6(2.2) K, $0.47(1)\mu_B$, respectively. We demonstrate that the Néel temperatures and the saturation hyperfine magnetic fields of the antiferromagnetically ordered Eu sublattice in both compounds are, respectively, 44.4(5) K, 294.2(7) kOe, and 43.5(1) K, 290.5(1) kOe. These findings show that a minimal substitution of Fe by Ni in $EuFeAs_2$, apart from inducing superconductivity in $EuFe_{0.97}Ni_{0.03}As_2$, dramatically diminishes the strength of the magnetism of the Fe sublattice and has virtually no effect on the magnetism of the Eu sublattice. The presence of antiferromagnetically ordered Fe and Eu sublattices in $EuFe_{0.97}Ni_{0.03}As_2$ proves that superconductivity and magnetism coexist in this compound. We observe that the increase of the magnitude of the main component of the electric field gradient tensor, at both Fe and Eu sites, with decreasing temperature is explained by a $T^{3/2}$ power-law relation. We determine the Debye temperatures of $EuFeAs_2$, $EuFe_{0.97}Ni_{0.03}As_2$, and the $FeAs_2$ impurity phase to be 355(18), 428(14), and 594(25) K, respectively.

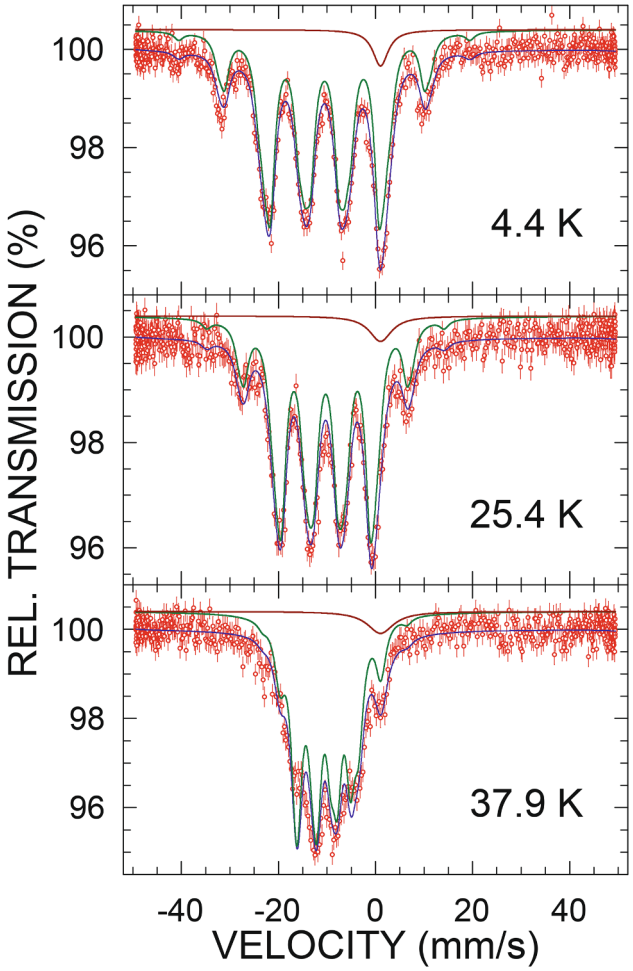

Fig. 23. ^{151}Eu Mössbauer spectra of $EuFe_{0.97}Ni_{0.03}As_2$ at the indicated temperatures fitted in the same way as the spectra in Fig. 12. The zero-velocity origin is relative to the source.

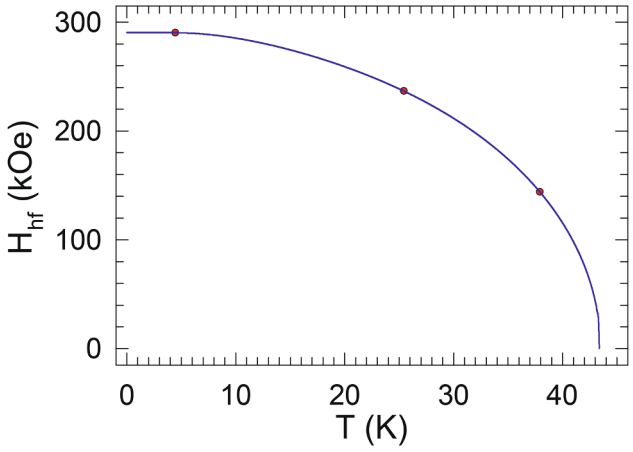

Fig. 24. Temperature dependence of the hyperfine magnetic field H_{hf} at ^{151}Eu nuclei determined from the fits of the spectra in Fig. 23. The solid line is the fit to Eq. (5), as explained in the text.

Author statement

Authors contributed equally to this work.

Declaration of Competing Interest

The authors declare that they have no known competing financial interests or personal relationships that could have appeared to influence the work reported in this paper.

Acknowledgments

This work was supported by the Natural Sciences and Engineering Research Council of Canada and the National Key Research and Development Program of China (Grant No. 2016YFA0300202).

References

[1] J. Yu, T. Liu, B.-J. Pan, B.-B. Ruan, X.-C. Wang, Q.-G. Mu, K. Zhao, G.-F. Chen, Z.-A. Ren, Sci. Bull. 62 (2017) 218.
[2] H. Yakita, H. Ogino, T. Okada, A. Yamamoto, K. Kishio, T. Tohei, Y. Ikuhara, Y. Gotoh, H. Fujihisa, K. Kataoka, H. Eisaki, J. Shimoyama, J. Am. Chem. Soc. 136 (2014) 846.
[3] J. Yu, T. Liu, K. Zhao, B.-J. Pan, Q.-G. Mu, B.-B. Ruan, Z.-A. Ren, Acta Phys. Sin. 67 (2018) 207403.
[4] Y.-B. Liu, Y. Liu, W.-H. Jiao, Z. Ren, G.-H. Cao, Sci. China-Phys. Mech. Astron. 61 (2018) 127405.
[5] G.-H. Cao (private communication).
[6] R. Street, B.C. Munday, B. Window, I.R. Williams, J. Appl. Phys. 39 (1968) 1050.
[7] J. Cieślak, S.M. Dubiel, Nucl. Instrum. Meth. Phys. Res. B 95 (1995) 131 and references therein.
[8] P. Bonville, F. Rullier-Albenque, D. Colson, A. Forget, EPL 89 (2010) 67008.
[9] P. Wang, Z.M. Stadnik, J. Żukrowski, A. Thaler, S.L. Bud'ko, P.C. Canfield, Phys. Rev. B 84 (2011) 024509.
[10] N.N. Greenwood, T.C. Gibb, Mössbauer Spectroscopy, Mössbauer Spectroscopy and Transition Metal Chemistry, Springer, Berlin, 2011.
[11] M.A. Albedah, F. Nejadsattari, Z.M. Stadnik, Y. Liu, G.-H. Cao, J. Phys.: Condens. Matter 30 (2018) 155803.
[12] P. Imbert, A. Gérard, and M. Wintenberger, CR Acad. Sci. (France) 256 (1963) 439; M. Yuzuri, R. Tahara, and Y. Nakamura, J. Phys. Soc. Jpn. 48 (1980) 1937.
[13] P. Panissod, J. Durand, J.I. Budnik, Nucl. Instrum. Meth. 199 (1982) 99; P. Panissod, Hyperfine Interact. 24-26 (1985) 607; O. Eriksson, A. Svane, J. Phys.: Condens. Matter 1 (1989) 1589; S.M. Dubiel, J. Alloys Compd. 488 (2009) 18.
[14] F. Grandjean, G.L. Long, in: G.J. Long, F. Grandjean (Eds.), Mössbauer Spectroscopy Applied to Inorganic Chemistry, Plenum, New York, 1989, vol. 3, p. 513.
[15] M.A. Albedah, K. Al-Qadi, Z.M. Stadnik, J. Przewoźnik, J. Alloys Compd. 613 (2014) 344.
[16] M.A. Albedah, F. Nejadsattari, Z.M. Stadnik, Y. Liu, G.-H. Cao, Phys. Rev. B 97 (2018) 144426 and references therein.
[17] D. Torumba, K. Parlinski, M. Rots, S. Cottenier, Phys. Rev. B 74 (2006) 144306.
[18] N.W. Ashcroft, N.D. Mermin, Solid State Physics, Saunders, Philadelphia, 1976.
[19] I. Nowik, B.D. Dunlap, J.H. Wernick, Phys. Rev. B 8 (1973) 238.
[20] W. Zinn, J. de Physique, Colloque, 32 (1971) C1-724; Ch. Sauer, U. Köbler, W. Zinn, G.M. Kalvius, J. de Physique, Colloque, 35 (1974) C6-269; G. Czjzek, V. Oestreich, H. Schmidt, K. Łątka, K. Tomala, J. Magn. Magn. Mater. 42 (1989) 79; I. Nowik, Y. Levi, I. Felner, E.R. Bauminger, J. Magn. Magn. Mater. 147 (1995) 373.
[21] I. Nowik, I. Felner, Z. Ren, G.H. Cao, Z.A. Xu, J. Phys.: Condens. Matter 23 (2011) 065701.